

Corrosion of Copper as a Nuclear Waste Container Material in Simulated Anoxic Granitic Groundwater

Xihua He,^{†,*} Tae Ahn,^{**} and Jin-Ping Gwo^{**}

ABSTRACT

Copper (Cu) is a candidate material for waste packages in geological disposal systems for high-level radioactive waste in Switzerland, Sweden, Finland, Japan, and Canada. This paper reports experimental tests of Cu in the context of radioactive waste disposal applications. Experimental tests of Cu general corrosion and hydrogen evolution were conducted under anoxic conditions (less than 10 ppb of O₂) using synthetic saline groundwater based on reference compositions of deep groundwaters in crystalline rock of the Canadian Shield. The results indicate that the Cu open-circuit potential and corrosion rates in anoxic waters were very sensitive to the residual O₂ concentration in solution. The corrosion rates ranged from submicrometer to micrometer per year, depending on the residual O₂ concentration level. The corrosion products were predominantly cuprous oxide (Cu₂O). Chlorine was present in corrosion products for tests exposed to synthetic saline groundwater, but more work is needed to assess its role in the corrosion process. Minute amounts of hydrogen were detected from the autoclave as test cell, however, they cannot be simply correlated to Cu corrosion because of complication of the autoclave material corrosion.

KEY WORDS: anoxic conditions, copper, corrosion, granitic groundwater, hydrogen evolution, nuclear waste package

INTRODUCTION

Some countries have been exploring the feasibility of generic high-level waste disposal at deep, geologic repositories in host rocks such as granite. The aqueous environments of these repositories contain a very low level of oxygen concentration in the groundwater. Copper (Cu) is a candidate container metal because Cu corrosion rate is very low in these environments. For the same reason, Cu has also been proposed for use as a waste package material in a number of high-level radioactive waste repository programs in other countries, including those in Switzerland, Sweden, Finland, Japan, and Canada.¹ In the past 20 y to 30 y, there has been considerable work on the corrosion of Cu in potential repository environments. Actively investigated areas include: (i) general corrosion and localized corrosion in the early oxidizing period, (ii) general corrosion in an oxygen (O₂)-free environment with hydrogen sulfide anion (HS⁻) and in O₂-free pure water without HS⁻, and (iii) performance of thin Cu coatings formed by cold spray or electrodeposition compared to wrought Cu.²⁻⁷

In the early period after repository closure, oxygen is expected to be present and the dose rate from radiation is higher than that at later period as fuel ages. This period could last tens to hundreds of years, depending on the repository design and characteristics of the spent nuclear fuel. According to the Pourbaix thermodynamic stability diagram,⁸ in the presence of an oxidant, typically O₂, corrosion of copper is likely to occur because the H₂O/O₂ equilibrium potential represented by line b in the Pourbaix diagram

Submitted for publication: April 7, 2017. Revised and accepted: August 22, 2017. Preprint available online: August 22, 2017, <https://doi.org/10.5006/2471>.

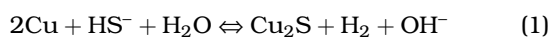
[†] Corresponding author. E-mail: xhe@swri.org.

^{*} Center for Nuclear Waste Regulatory Analyses, 6220 Culebra Road, San Antonio, Texas 78238.

^{**} U.S. Nuclear Regulatory Commission, Washington, DC 20555-0001.

is above the Cu/Cu^+ , $\text{Cu}^+/\text{Cu}^{2+}$, or Cu/Cu^{2+} equilibrium potential. In this case, O_2 functions as an acceptor for the electrons produced by copper oxidation. In oxic conditions, Cu corrosion behavior has been well studied and a large database is available in the literature. Corrosion rates vary depending on the O_2 concentration in solution, and are predominantly in the range of tens of micrometers to a few micrometers per year. During the early oxidizing period, γ radiation may produce nitric acid (HNO_3), oxidants such as hydrogen peroxide, and hydrogen (H_2). Lousada, et al.,² report that γ radiation at a total dose of 69 kGy enhances hydrogen absorption in Cu significantly compared to absorption into unirradiated Cu, and the amount of hydrogen absorbed depends on the accumulated radiation dose to the Cu metal. Localized corrosion may also occur during this early oxidizing period, when oxidants are present to drive Cu dissolution. Researchers have shown that localized corrosion of Cu may be limited to surface roughening or under-deposit corrosion (rather than pitting) because factors that contribute to repassivation are commonly established for Cu. Of the corrosion allowance estimate of 1.27 mm over a million years developed by the Canadian nuclear waste management disposal program, only 0.1 mm was estimated to be a result of under-deposit corrosion.³

At a later period, the groundwater contacting the waste packages is expected to be depleted of O_2 , but could contain HS^- , Cl^- , SO_4^{2-} , and H_2CO_3 in solution. HS^- is usually produced from two sources: (i) sulfate reducing bacteria and (ii) dissolution of pyrite (FeS_2).⁴ According to the Pourbaix diagram, HS^- enhances Cu reaction with anoxic water forming a Cu_2S film through the following reaction:



The depth of the corrosion front resulting from the reaction of Cu with HS^- depends on the rate of supply of HS^- present in the groundwater, and on the copper (I) sulfide (Cu_2S) film properties including chloride (Cl^-) effects. Taniguchi and Kawasaki⁵ measured Cu corrosion rates in anoxic synthetic seawater with added sodium sulfide (Na_2S) using the weight loss method. The corrosion rate increased from less than 0.6 $\mu\text{m}/\text{y}$, to 2 to 4 $\mu\text{m}/\text{y}$, to 10 to 15 $\mu\text{m}/\text{y}$ as sulfide (S^{2-}) concentration increased stepwise from 0.001 M to 0.005 M to 0.1 M, respectively. In the absence of S^{2-} , the average corrosion rate was estimated to be 0.088 $\mu\text{m}/\text{y}$ over a test period of nearly 800 d. SKB⁴ considered Cu reaction with HS^- in a repository environment, but this reaction was concluded to be non-risk significant in SKB's safety assessment on the basis of analyses assuming instant HS^- reaction with Cu as soon as it reaches the waste canister surface and limited equivalent groundwater flow rates. In the SKB analyses the corrosion depth was controlled by the rate of supply of HS^- dissolved in groundwater, and was

estimated to be less than 100 μm in 1 million years (assuming well-spread damage over the waste package surface). After depletion of both O_2 and HS^- in buffer and backfill materials, Cu could predominantly react with water through the following reaction (as the rate of supply of HS^- in groundwater is highly constrained):



According to the Pourbaix diagram, Cu is thermodynamically stable in O_2 -free environments because the H^+/H_2 equilibrium potential is lower than the Cu^+/Cu and Cu^{2+}/Cu equilibrium potential, except at some extreme conditions that the equilibrium potentials change order.⁸ However, Cu thermodynamic stability has been long debated⁹⁻¹² and remains as an area of interest. Given few Cu corrosion studies in O_2 -free environments, the debate in the literature on Cu stability, and the possibility of long-term exposure of Cu to anoxic and high-salinity groundwaters in repository settings, further research is warranted. This paper focuses on assessing Cu general corrosion and H_2 detection in simulated granitic groundwater and pure water. The O_2 concentration in the aqueous phase is maintained as low as possible through inert gas deaeration.⁶⁻⁷

EXPERIMENTAL APPROACHES

Simulated Granitic Groundwater

Groundwaters in crystalline rocks are generally reducing with increasing salinity with depth.¹³ At a nominal repository depth (e.g., 500 m), groundwaters may be at or near thermodynamic equilibrium with secondary mineral phases such as calcite (calcium carbonate) or gypsum (calcium sulfate), though dissolved carbonate (CO_3^{2-}) and sulfate (SO_4^{2-}) concentrations are also typically present but at low concentrations. For example, SO_4^{2-} concentrations in Swedish groundwater samples from nominal repository depths range from near 0 mg/L to approximately 600 mg/L.¹⁴

Designs for a repository constructed in granitic host rocks call for an engineered barrier such as sodium (Na)-bentonite, a swelling clay material, as a barrier against groundwater flow and radionuclide release (in case of failure of canisters to isolate the radioactive waste).³⁻⁴ As groundwater saturates and reacts with the bentonite, dissolution and ion exchange reactions initially will alter the composition of the near-field groundwater contacting the container and, if the container fails, that of the water contacting the spent fuel waste form. For example, ion exchange reactions between Na-bentonite and the contacting calcium (Ca)-rich water are likely to increase the dissolved Na concentration and decrease the dissolved Ca concentration in the water. If the bentonite also contains some gypsum ($\text{CaSO}_4 \cdot 2\text{H}_2\text{O}$), its dissolution will tend to increase the concentration of sulfate ions. These

changes are pronounced during the early stages of saturation of the bentonite. As additional pore volumes of groundwater move through the bentonite over time, the near-field water chemistry will gradually evolve toward a composition more similar to that of the surrounding groundwater.

For the Cu corrosion experiments in this study, a solution composition was selected to be representative of a deep groundwater chemistry that is likely to occur at nominal repository depths in a massive crystalline bedrock such as granite.¹⁵ The solution composition is based on reference Canadian Shield groundwater compositions,¹⁶⁻¹⁷ particularly the reference synthetic groundwater WN-1m, initially developed for use in sorption experiments from groundwater data collected over depths between 350 m and 800 m below the surface.¹⁶ The WN-1m composition is in the mid-range of concentration values for analyzed Canadian Shield groundwaters at depth,¹⁸ and it is at or near equilibrium with calcite. The simulated groundwater composition for this study and similar compositions¹⁶⁻¹⁷ are listed in Table 1.

The chemical reagents, sodium chloride (NaCl), potassium chloride (KCl), sodium sulfate (Na₂SO₄), calcium chloride (CaCl₂), magnesium chloride (MgCl₂·6H₂O), and sodium bicarbonate (NaHCO₃), were used to prepare this simulated groundwater. The pH, measured by a pH meter, was 6.65 at ambient temperature and atmospheric condition before deaeration.

O₂ Concentration Measurement

This work was aimed at establishing an anoxic environment. In all of the tests, the simulated granitic groundwater was deaerated with argon (Ar) gas overnight before immersing the test specimen and deaerated continuously throughout the test except for the tests in air-tight autoclaves. O₂ concentration in the solution was measured and monitored with an O₂ probe and O₂ meter purchased from Oakton Instruments.¹⁹ The probe works on a galvanic principle and consists of a cathode, anode, and an inner electrolyte. At the cathode, O₂ is electrochemically reduced to hydroxyl ions, producing an electrical current within the probe proportional to the O₂ concentration. The O₂ measurement range for the probe is 0 ppm to 20 ppm with resolution of 10 ppb.¹⁹ After deaerating the solution overnight, the probe indicated that the O₂ concentration was zero. At this zero reading, according to the instrument resolution limitation, the O₂ concentration is interpreted to be below 10 ppb. With continuous purging during the test, the meter remained at the zero reading. Some tests were set up

TABLE 1
Comparison of Three Reference Groundwaters for Deep Crystalline Rocks

Species	Concentration (M)		
	Reference Simulated Groundwater (This Study)	Synthetic Groundwater WN-1m ¹⁶	Reference Deep Groundwater CR-10 ¹⁷
Na ⁺	8.0 × 10 ⁻²	8.0 × 10 ⁻²	8.0 × 10 ⁻²
Ca ²⁺	1.0 × 10 ⁻²	5.0 × 10 ⁻²	5.0 × 10 ⁻²
Mg ²⁺	3.0 × 10 ⁻³	3.0 × 10 ⁻³	2.5 × 10 ⁻³
K ⁺	4.0 × 10 ⁻⁴	4.0 × 10 ⁻⁴	3.8 × 10 ⁻⁴
Cl ⁻	9.2 × 10 ⁻²	2.0 × 10 ⁻¹	2.0 × 10 ⁻¹
SO ₄ ²⁻	7.0 × 10 ⁻³	9.0 × 10 ⁻³	1.0 × 10 ⁻²
HCO ₃ ⁻	8.9 × 10 ⁻⁴	1.0 × 10 ⁻³	1.1 × 10 ⁻³

in an Ar-purged glovebox, during tests in which the O₂ concentration was also monitored.

An optical probe was used to confirm the low O₂ concentration. The optical probe is based on the O₂-dependent luminescence quenching principle. The measurement range for the probe is 4 ppb to 25 ppm with an accuracy of 0.05 vol% at low O₂ concentrations.²⁰ The probe was set next to the location where the galvanic probe was located. Instead of reading zero, the O₂ concentration was measurable at both locations, but was <10 ppb.

Open-Circuit Potential and Electrochemical Measurement at 50°C and 80°C

The open-circuit potential (OCP) was measured with the Cu electrodes immersed in the simulated granitic groundwater at 50°C and 80°C. Electrochemical impedance spectroscopy (EIS) and linear polarization resistance (LPR) were used to measure corrosion rates. Cylindrical electrodes of 6.3 mm diameter and 50 mm length machined from oxygen-free high-conductivity pure Cu rods (99.99% Cu UNS C10100⁽¹⁾ purchased from Alfa Aesar[®]) were used as working electrodes in the tests. A 2 L glass cell equipped with a gas bubbler for deaerating, a condenser, a saturated calomel reference electrode (SCE), a platinum counter electrode, and a thermowell were used in the test. The solution was deaerated with Ar before and during the test. Some of the tests were performed with the deaerated cells set up in an ambient air environment. All of the fittings for electrodes and other accessories penetrating through the cell lid were wrapped with polytetrafluoroethylene (PTFE) tape to minimize air entry. For some tests, the same type of deaerated cell was set up in an Ar-purged glovebox (Figure 1) to further reduce the O₂ concentration.

EIS was conducted at the OCP, applying a 10 mV amplitude sinusoidal wave. An equivalent electric circuit was fit to the EIS data to derive the polarization resistance, R_p. LPR was performed between -10 mV_{OCP} and 10 mV_{OCP} with a scanning rate of 0.167 mV/S.

⁽¹⁾ UNS numbers are listed in *Metals and Alloys in the Unified Numbering System*, published by the Society of Automotive Engineers (SAE International) and cosponsored by ASTM International.

[†] Trade name.

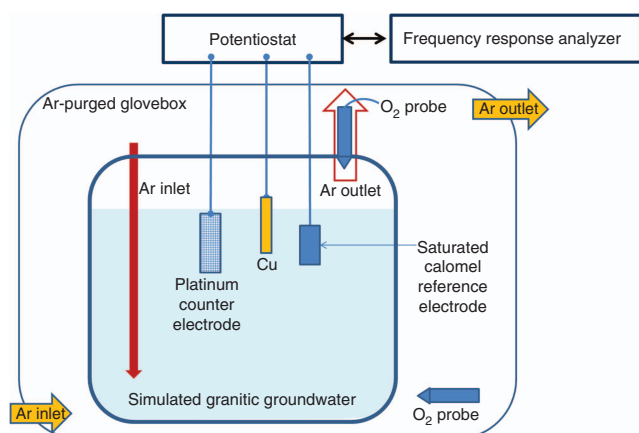


FIGURE 1. Glass cell for Cu exposed to Ar-deaerated simulated granitic groundwater set up in an Ar-purged glovebox.

A linear fit approximating the LPR data was used to compute the R_p . The corrosion rate was calculated in accordance with ASTM G102²¹ from the R_p derived from both EIS and LPR assuming that (i) the current distributes uniformly across the surface area exposed to the solution, (ii) both the anodic and cathodic beta Tafel constants are 120 mV/decade (i.e., the Stern-Gearly constant is 0.027 V/decade), and (iii) the Cu equivalent weight was 64 g (i.e., the valence of the copper after oxidation in the corrosion process is +1). The Cu density used in the calculation was 8.96 g/cm³.

Cu Exposed in Autoclave at 80°C for H₂ Concentration Measurement

Gas was collected from the head space of a sealed autoclave and the H₂ concentration was quantified to determine any hydrogen release or production. Cu foil purchased from Alfa Aesar^{®†} was used in the test. The foil was 0.25 mm thick, annealed, oxygen-free, and had a Cu concentration of 99.997%. Hydrogen content in the material was not reported in the Certificate of Analysis provided by the supplier because it was not analyzed. Instead, independent analysis of hydrogen content in the as-received Cu foil was performed by two accredited laboratories using inert gas fusion method with detection limit of 0.6 ppm.²² The hydrogen content was consistently determined to be 5±1 ppm. Immediately before the test, the foil was polished with SiC paper up to 600 grit, cleaned with deionized water in ultrasonic cleaner, and dried with acetone. No heat treatment was done on the material.

The autoclave cylinder and head were made from a nickel-based super alloy and Type 316 stainless steel (UNS S31600), respectively. A PTFE liner was set inside the cylinder to avoid direct solution contact with the nickel alloy. The volume of the autoclave was 2.1 L and the solution amount was 1.2 L. Before immersing the materials in solution, the solution was deaerated in a glovebox purged by inert gas. After both the O₂

concentration in the solution and the glovebox reached a reading of 0, the autoclave was sealed in the glovebox to achieve anoxic condition. The pressure vessel lid was fit with a thermowell and a calibrated pressure gauge for temperature and pressure monitoring. A needle valve for gas sampling and a pressure relief valve were connected to the autoclave. All of the tests in autoclave were conducted at 80°C.

The tests started at two different internal pressures applied by the inert gas: 1 atm and 3 atm (101.325 kPa and 303.975 kPa), where the quantity of the inert gas sealed at the head space was estimated to be 0.037 mol and 0.11 mol, respectively. Another test with pure water was set up at 3 atm under the same condition in the Ar-purged glovebox. After 3 months, gas was sampled from the head space of each autoclave through the valve using Tedlar^{®†} gas sampling bags and analyzed for H₂ concentration with HP 5890[†] gas chromatography (GC) immediately after sampling. The GC uses a pulsed discharge helium ionization detector and helium as the carrier gas. It was calibrated before each measurement using ultra high purity UHP grade (99.995%) N₂ diluted with different amount of H₂. A 4-point or 5-point calibration curve was used to calculate the concentration of H₂ in samples. The GC instrument has a H₂ detection limit of 0.002 vol%.

For the test at 3 atm, after gas sampling, the autoclave was cooled down to room temperature and then repressurized to 3 atm with Ar gas through the gas inlet in the Ar-purged glovebox to ensure no O₂ entry into the cell. Another gas sample was taken at the end of the test, at about 6 months. During the test, to ensure a good seal, the temperature and pressure were checked daily. For the test in simulated granitic groundwater at 1 atm, three post-test Cu foils were analyzed for hydrogen content along with one untested specimen. For the test in simulated granitic groundwater at 3 atm, the corrosion products on the post-test Cu foils were cleaned off using the deaerated cleaning solution (500 mL HCl mixed with 500 mL water) for 1 min to 3 min at room temperature following specification in ASTM G1 for weight loss analysis.²³

RESULTS

Open-Circuit Potential

Figure 2(a) compares the OCP of Cu measured from an Ar-deaerated cell set up in air and the other set up in the Ar-purged glovebox at 50°C. For the cell set up in air, the OCP fluctuated between $-0.28 V_{SCE}$ and $-0.24 V_{SCE}$, without an evident trend in the OCP data. For the cell set up in the Ar-purged glovebox, the data were not continuous because the measurements were interrupted weekly for EIS measurement. After immersing the electrode in solution, the OCP was approximately $-0.28 V_{SCE}$ and it decreased with time. At day 10, the glovebox was opened to set up another

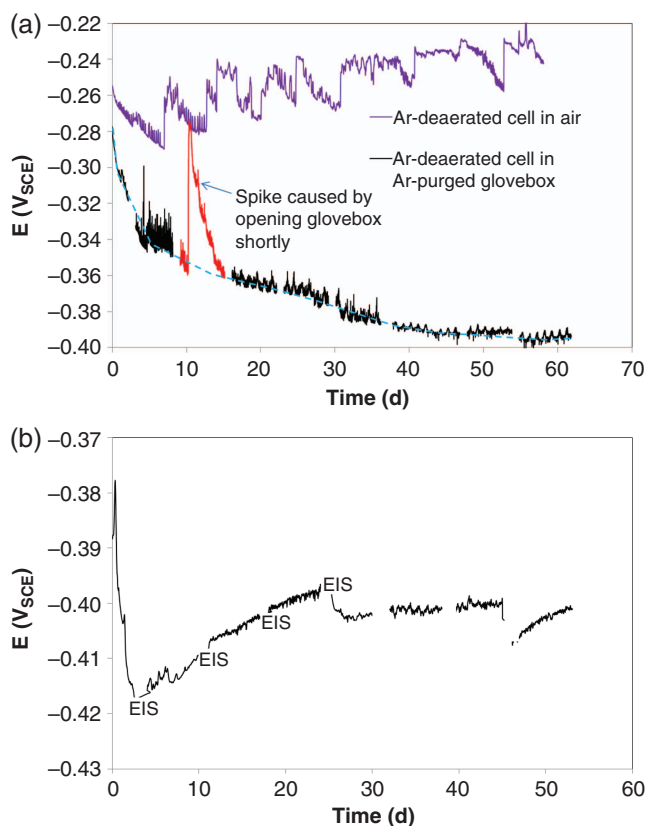


FIGURE 2. OCP of Cu exposed to Ar-deaerated simulated granitic water at (a) 50°C with the test cell set up in air and in Ar-purged glovebox and (b) 80°C with the test cell set up in Ar-purged glovebox.

test. Opening the glovebox caused a voltage spike, which shifted readings to a more positive OCP, eventually reaching the OCP measured from the cell set up in air. This indicates that the glass cell set up in ambient air was not air tight and that O₂ from the air entered the cell, although it was continuously purged with Ar. It

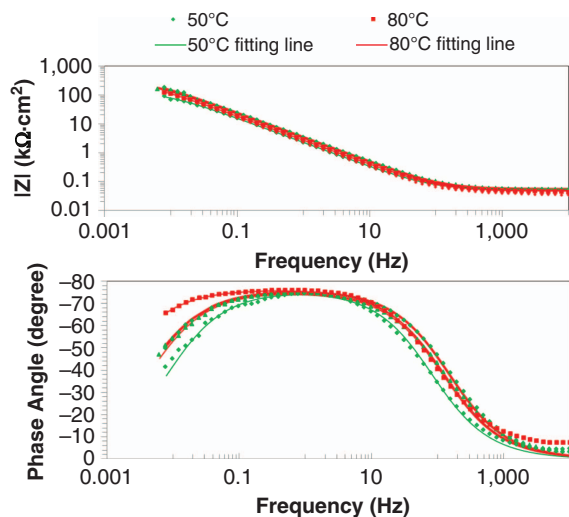
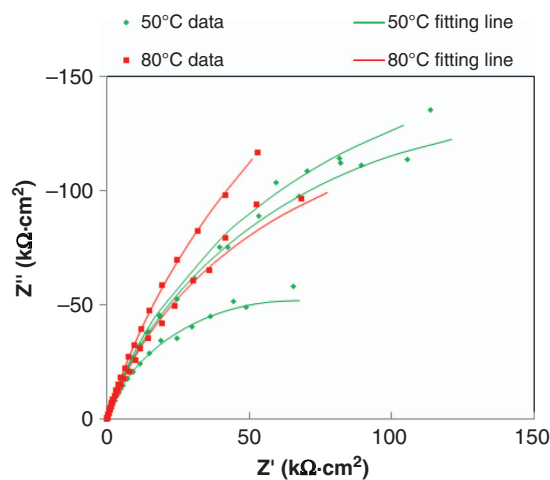


FIGURE 3. Nyquist and bode plots of EIS of Cu exposed to simulated anoxic granitic groundwater at 50°C and 80°C.

took approximately 5 d for the OCP to return to the original trend. In the following days, the OCP continued to decrease, but at a lower rate compared to the first 10 d. At day 64 when the test was ended, the OCP was approximately $-0.39 V_{SCE}$. The dotted line in the plot shows the general trend of the OCP. OCP decrease could be caused by the depletion of O₂ by corrosion. Another feature noted from the measurements is the daily fluctuation of the OCP. This could be caused by the temperature fluctuation of the test cell, as the temperature was controlled by on-and-off electric circuits.

Figure 2(b) shows the OCP data at 80°C for the cell set up in the Ar-purged glovebox. The measurement was also interrupted for EIS measurement. The OCP decreased to near $-0.42 V_{SCE}$, then increased back to about $-0.40 V_{SCE}$, which is close to the measurement at 50°C from the cell set up in the same environment. Different trends of OCP can be an effect of temperature on the corrosion process.

Electrochemical Impedance Spectroscopy and Linear Polarization Resistance Measured Corrosion Rates from Deaerated Cells Exposed to Air at 50°C and 80°C

The EIS data shown in Figure 3 had similar features, with one time constant sufficient to describe the impedance signature in the applied frequency range. A Randles electric circuit with one constant phase element was fit to the impedance data. The fitting lines are also plotted in Figure 3. The fitting error for all of the parameters was less than 10%. The corrosion rates computed from the derived polarization resistance are summarized in Table 2. They are on the order of several $\mu\text{m}/\text{y}$. Considering the data uncertainty, there is no clear trend of the corrosion rate on the temperature. The LPR measurement was performed after EIS. Figure 4 shows examples of the LPR curves

TABLE 2

Corrosion Rates of Cu Exposed to Deaerated Simulated Granitic Groundwater for Test Cells Exposed to Air

Temperature (°C)	50			80				
Corrosion rate ($\mu\text{m}/\text{y}$)	Test 1	EIS	0.83	0.95	2.4	1.0	0.48	
	Test 2	EIS	5.0	3.5	3.4	3.0	3.0	4.4
		LPR	5.3	5.1	4.9		6.7	
Average corrosion rate ($\mu\text{m}/\text{y}$)				3.5 \pm 1.8			3.1 \pm 2.3	

at 50°C and 80°C. Over the small polarization range, the current response is approximately linear, which allows the straight line to be fitted to the data to derive the polarization resistance using another electrochemical method. The corrosion rates calculated from the linear polarization curves are also included in Table 2. They were very close to those computed using EIS. The post-test specimen surface was tarnished with a black film in some areas. Examination under an optical microscope shows some localized features, but those features are too shallow to be characterized as pits.

Electrochemical Impedance Spectroscopy Measured Corrosion Rates in Simulated Granitic Groundwater from Cells Exposed to Inert Atmosphere at 50°C and 80°C

Figures 5(a) and (b) show the EIS data normalized with an electrode surface area of 7.28 cm² for the cell set up at 50°C exposed to an inert atmosphere. The OCP data are shown in Figure 2(a). Over the frequency range of the measurement, impedance signatures can be duplicated with an equivalent electrical circuit with one time constant. The fitting line for the data set at 8 d is shown in Figure 5(c) as an example. Fitting to other data sets was similar, but was not shown for clarity. The fitting error for R_p was the highest, which ranged from 5% to 25%. The polarization resistance, R_p , was computed by adjusting the parameters of the electrical circuit to fit the impedance signatures, which was then used to calculate the corrosion rate. Figure 6(a) plots the corrosion rate calculated from the EIS and electric circuit fits at 50°C. At 2 d, the corrosion rate was

above 1 $\mu\text{m}/\text{y}$, but it decreased with time to values below 1 $\mu\text{m}/\text{y}$. Figure 2(a) indicates that it took at least 5 d for the O₂ concentration to decrease to an extremely low level. The initially higher corrosion rate could be a result of larger amounts of residual O₂ in the solution. It is apparent that the corrosion rate would continue decreasing with time. However, given the EIS data fitting uncertainty, this decreasing trend could not be fully corroborated. The post-test Cu cylinder was discolored. Figure 6(b) shows the corrosion rates and post-test Cu at 80°C. The corrosion rate increased after 15 d and the overall corrosion rate was slightly higher than that observed at 50°C. The post-test Cu was also discolored.

H₂ Concentration Measurement and Corrosion Products for Cu Exposed to Simulated Granitic Groundwater and Pure Water in Autoclaves at 80°C

Test in 1 atm Inert Gas Pressure — The pressure of the autoclave increased with increasing temperature. After the autoclave temperature stabilized at 80°C, the pressure remained steady at 1.48 atm (149.961 kPa). The pressure increase corresponding to the temperature was primarily from two sources: (i) the pressure of the inert gas originally contained in the autoclave increased with rising temperature and (ii) water evaporated with increasing temperature. Using ideal gas law and the 0.9 L head space, the pressure increase from 20°C to 80°C is 0.20 atm (20.265 kPa) for original pressure at 1 atm, which is lower than the total recorded pressure increase. This means that water also

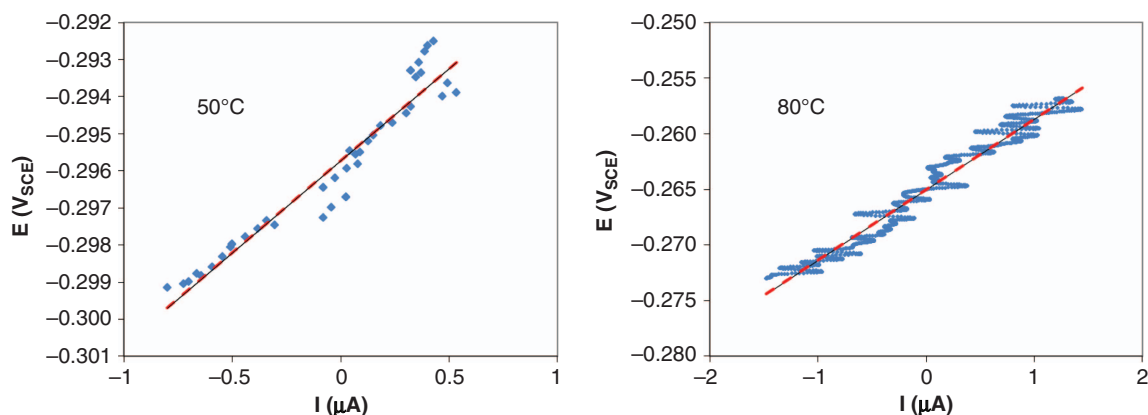


FIGURE 4. Examples of linear polarization curves of Cu exposed to anoxic simulated granitic groundwater at 50°C and 80°C.

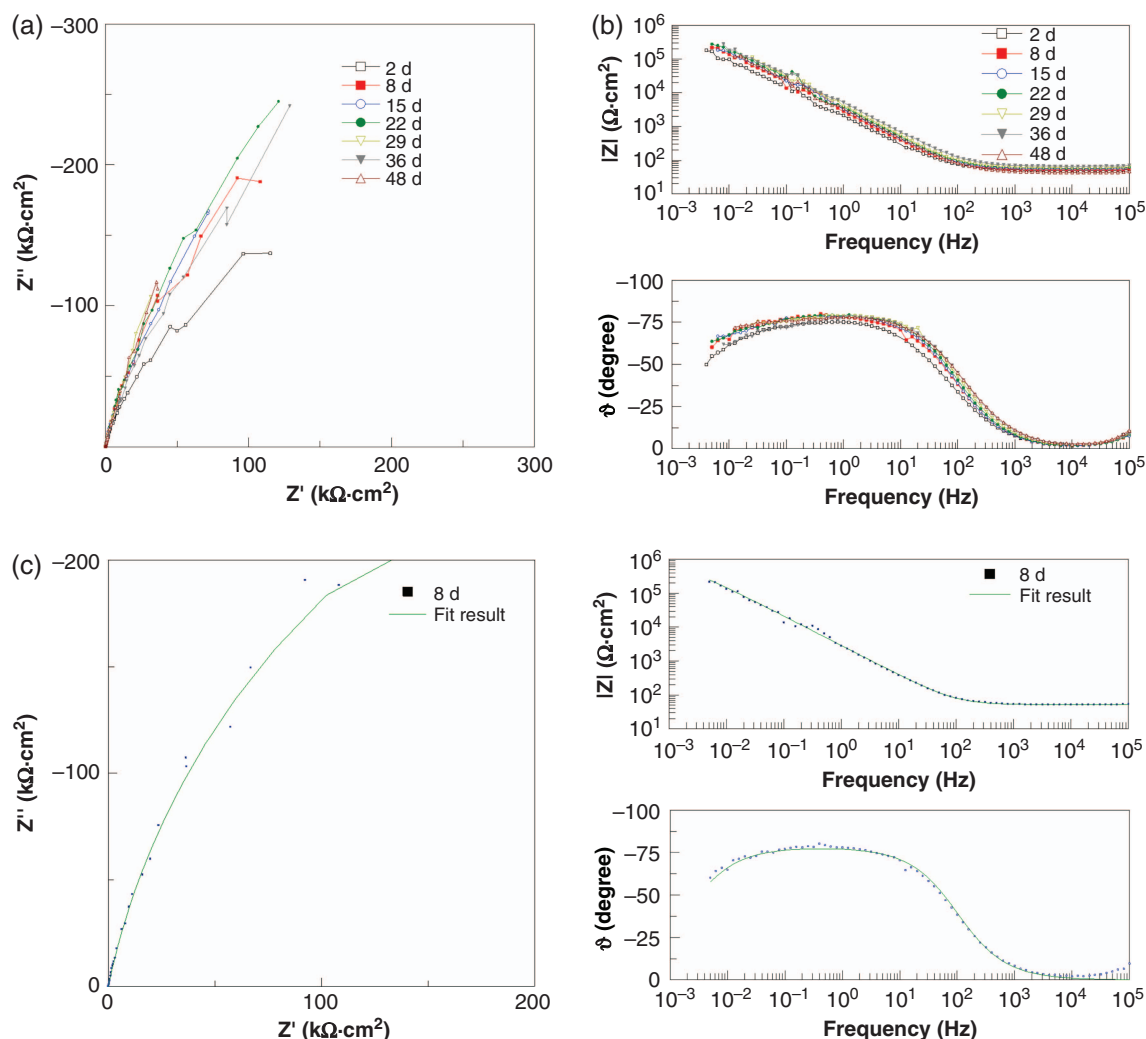


FIGURE 5. EIS of Cu exposed to Ar-deaerated simulated granitic groundwater: (a) Nyquist and (b) Bode plots at 50°C; (c) a fitting example.

evaporated into the head space at this temperature, which led to additional pressure increase of 0.28 atm. A thin film of liquid could be present on the autoclave inner wall surface.

Gas was sampled at 3 months and 6 months for H₂ concentration measurement using GC. After sampling, water vapor was condensed in the sampling bag. H₂ was detected in both samples. The H₂ concentrations were 0.18 vol% and 0.20 vol%, respectively. The test was stopped at 6 months. The post-test solution was still clear, but there was black powder at the bottom of the cell. The Cu foil also was tarnished with a black film in some areas. Three post-test Cu foils were analyzed for hydrogen content along with one base specimen. The tested specimens had hydrogen contents of 3±1 ppm, 3±1 ppm, and 5±1 ppm, which is the same as the untested specimen. Consistent results were obtained from another independent analysis.

Test in 3 atm Inert Gas Pressure — With the heating up of the autoclave, the pressure increased to 4.1 atm

(415.432 kPa) at 80°C. Using the ideal gas law and the 0.9 L head space, the pressure increase of the inert gas in the autoclave from 20°C to 80°C was 0.6 atm (60.795 kPa), which is lower than the total recorded pressure increase. This means that water still evaporated into the head space under the pressurized condition, which led to additional pressure increase of 0.5 atm (50.662 kPa) associated with water vapor. Gas was sampled from the head space of each autoclave at 3 months. The H₂ concentration was analyzed to be 0.02 vol%. The amount of H₂ was about 2.2×10^{-5} mol calculated from the volume percentage and the amount of inert gas in the autoclave. Another gas sample was taken at 6 months and the cell was opened to examine the Cu foil and solution. The Cu was analyzed for surface composition and the solution was collected to analyze the Cu concentration. The hydrogen concentration over the following 3 months was 0.02 vol%, which was the same as after the initial 3 months.

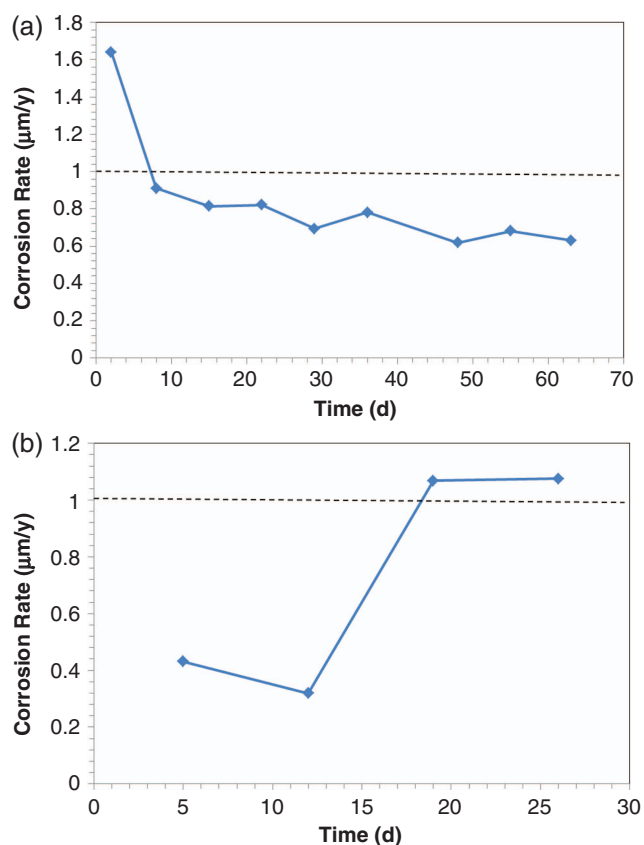


FIGURE 6. Post-test Cu cylindrical electrode after exposing to Ar-deaerated simulated granitic groundwater in equilibrium with inert atmosphere and EIS-measured corrosion rates at (a) 50°C and (b) 80°C.

Most of the area of the post-test Cu foils was still shiny, but some regions had reddish and blackish stains. The post-test solution looked clear, but there were some red and black corrosion products clinging to the PTFE liner wall. Some stains also were observed at the pressure vessel head and the thermowell wall. Some stains on the Cu foil were scraped off immediately from the Cu foil after the test and analyzed with x-ray diffraction (XRD) and energy dispersive x-ray spectroscopy (EDX). The XRD and EDX results are shown in Figure 7. XRD shows that the stain was predominantly Cu_2O , which is consistent with the red corrosion products on the Cu foil and consistent with the observation.²⁴ Both CuO and CuS are black, but the EDX in Figure 7(b) shows that there is no sulfur detected on the Cu surface. This indicates that the black corrosion products observed on the Cu foil is CuO, not CuS. However, any quantity of CuS could have been too low to have been detected by XRD. In addition to the Cu detected from the scraped-off stains using EDX, silicon, chlorine, calcium, carbon, and oxygen also were detected. Calcium and carbon could come from solution deposition, while silicon could be residue from SiC paper polishing. The presence of chlorine in the oxide could indicate involvement of chloride in the

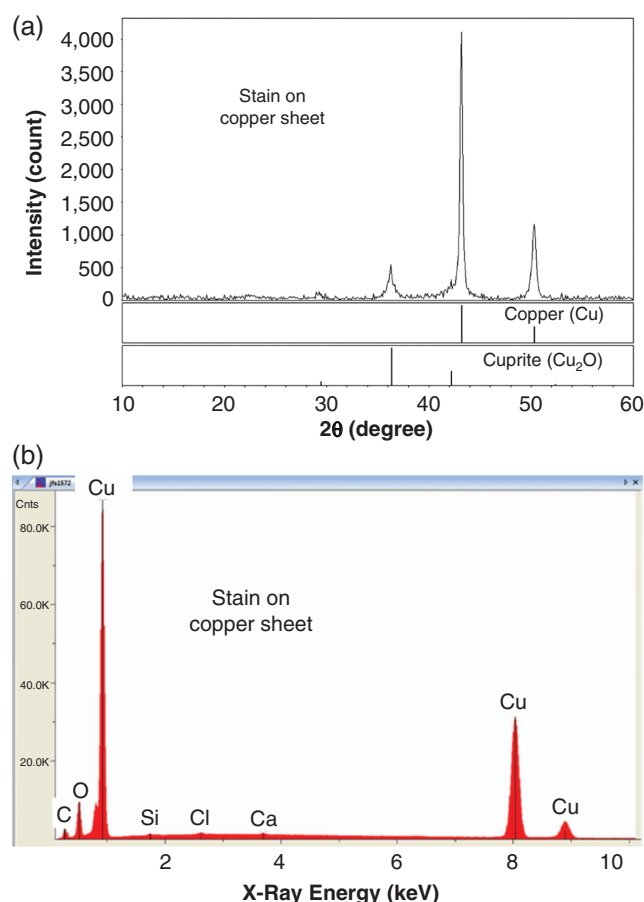


FIGURE 7. (a) X-ray diffraction and (b) energy dispersive x-ray spectroscopy of stains scraped off from post-test Cu foils.

corrosion process, but more work is needed in assessing its role.

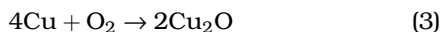
Liquid samples were analyzed for dissolved copper using the inductive coupled plasma atomic emission spectroscopy method. For the tests with Cu specimens, the copper concentration was 1.41 ppm, which is well above the instrument detection limit of 0.005 ppm. These results indicate that some Cu corroded and dissolved in solution. The amount of copper was calculated to be 2.6×10^{-5} mol over the test duration of 6 months, which is less than the total amount of H_2 detected over the same test duration.

Cu Corrosion Rates from Weight Loss

The Cu foil had a total weight loss of 0.05048 g after cleaning from the test. This was equivalent to 89 nm metal loss averaged over the entire surface area of 631 cm^2 using a Cu density of 8.96 g/cm^3 . The metal loss could be from two sources: (i) Cu consumption by residual O_2 (from the incomplete deaeration) and (ii) Cu corrosion in O_2 -free water.

Assuming the residual O_2 concentration in the 2 L vessel from incomplete deaeration is 10 ppb, which is the resolution of the Oakton[†] O_2 probe, and assuming Cu reacts with O_2 through Reaction (3), the

consumption of Cu by residual O₂ was estimated to be 0.28 nm, which is only 0.3 percent of the overall metal loss. This suggests that Cu consumption by residual O₂ is significantly less than Cu corrosion in O₂-free water. Thus, the entire weight loss was used to estimate the average corrosion rate over 6 months, which is equal to 0.2 μm/y. This corrosion rate is in the same range as the majority of the instantaneous corrosion rate computed with EIS data, shown in Figure 6.



H₂ Concentration Measurement for Cu Exposed to Deaerated Pure Water in Autoclave at 80°C

The test was terminated after 204 d. At 3 months and the end of the test, vapor phase was sampled and the H₂ concentration was analyzed. The H₂ concentration was 0.004 vol% and 0.005 vol%. Most of the post-test Cu foil surface was oxidized. The XRD and EDX results of the oxidation products on the Cu foil are shown in Figure 8. XRD shows that the oxide is predominantly Cu₂O, which is consistent with the composition in Figure 7(a). In addition to Cu shown by EDX, very small amounts of aluminum, silicon, carbon, and oxygen were detected. Carbon could come from air exposure, while aluminum and silicon could be

residue from SiC paper polishing. As expected, no chlorine was detected on the surface.

DISCUSSION

Effects of Residual O₂ in Anoxic Solution on Cu Corrosion

The comparison of OCP in Figure 2 from the two cells indicates that the trend is different for cells set up in air and in an inert atmosphere. For cells exposed to air, more O₂ was available, leading to higher OCP. For cells exposed to an inert atmosphere, the Ar gas forms a blanket around the cell, which makes it more difficult for O₂ to diffuse into the cell, leading to lower and continuously decreasing OCP. The data in Figure 6(a) show that the corrosion rate measured from the cell set up in the glovebox was almost one order of magnitude lower than that measured with the cell surrounded by air (Table 2). O₂ penetration into the cell could have contributed to the higher OCP, leading to higher corrosion rates. The dependence of corrosion rate and OCP on O₂ concentration is consistent with other studies showing that the Cu corrosion rate is sensitive to O₂ concentration. King and Watson²⁵ measured the dependence of Cu corrosion rates in compacted clay on the salinity of the groundwater. The corrosion rates increased with increasing O₂ concentration, but decreased with increasing Cl⁻ concentration. In the presence of O₂ or some oxidants, Cu undergoes general corrosion as a result of the anodic dissolution of Cu coupled to the reduction of a suitable oxidant, such as dissolved O₂ or Cu(II) ions. In chloride-dominated environments in the presence of O₂, Cu dissolves as Cu(I) with the formation of dissolved CuCl₂ ions, along with precipitated Cu₂O and CuCl₂·3Cu(OH)₂.²⁶ King and Watson²⁵ showed that at a low O₂ concentration, the corrosion rate is of the order of several micrometers per year, which is similar to the corrosion rates shown in Table 2. The corrosion rate values in Table 2 are also close to measurements in literature.²⁷⁻²⁸

Kosec, et al.,²⁶ investigated Cu corrosion rates in oxic environments using thin electrical resistance sensors placed in a test package containing bentonite and saline groundwater at room temperature for 4 y. Additionally, the corrosion rate was monitored by EIS measurements on the same sensors. By the end of the exposure period, the corrosion rate was estimated to have dropped to approximately 1.0 μm/y and the corrosion products were determined to be Cu₂O and paratacamite. These are also consistent with the corrosion rate values in Table 2 and the corrosion products shown in Figures 7 and 8.

The corrosion rate values in Table 2 were significantly higher than those predicted based on kinetic modelling of bentonite-Cu canister interaction²⁹ and those measured in pure water based on H₂ generation. According to the Pourbaix diagram, Cu is thermodynamically stable in O₂-free environments. In anoxic

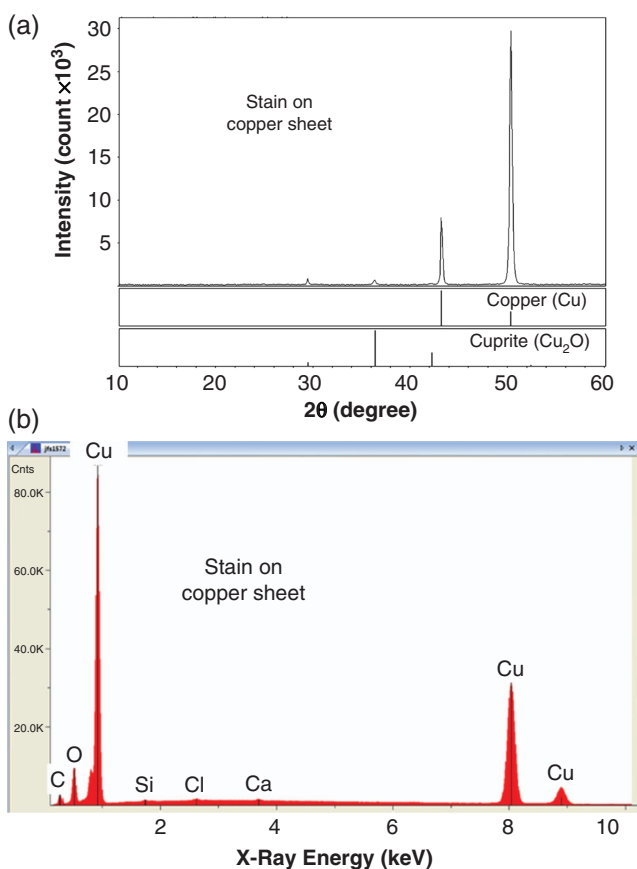


FIGURE 8. (a) X-ray diffraction and (b) energy dispersive x-ray spectroscopy of post-test Cu foils.

conditions, researchers reported lower and upper bounds for corrosion rates of $0.0001 \mu\text{m}/\text{y}$ and $0.02 \mu\text{m}/\text{y}$, respectively.²⁹ The corrosion depth was estimated to be less than $120 \mu\text{m}$ over one million years assuming a low equilibrium H_2 pressure of 0.001 bar (0.1 kPa) and limited transport of H_2 away from the waste container.⁴ A Canadian nuclear waste management program study estimated a penetration depth of the corrosion front of 1.27 mm over a million year disposal period, in which only 0.17 mm was from general corrosion.³ This suggests that the general corrosion rate used in the analyses was less than a few nanometers per year, similar to corrosion rates considered.⁴ These corrosion rate values derived based on thermodynamics assumed a completely O_2 -free environment, in contrast to this experimental study, in which O_2 in solution was stripped by deaerating with inert gas. The extent of O_2 depletion would depend on O_2 partial pressure in the surrounding environment (based on Henry's law). Some trace amount of O_2 could still remain in solution in the experiments, which could account for the higher measured corrosion rates compared to kinetic modeling. Furthermore, other chemical species such as chloride and sulfate in the simulated granitic groundwater used in this study could also have caused the different corrosion rates.

Analysis of H_2 Evolved from Tests in Autoclave

According to the corrosion reaction in Equation (2), the corrosion rate can be estimated based on the amount of H_2 produced. Therefore, researchers have attempted to measure the amount of H_2 produced to indirectly determine the thermodynamic stability of Cu in anoxic water. Boman, et al.,²⁷ performed Cu immersion tests in pure water in autoclaves alongside tests with two reference cells without Cu. Prior to the tests, the Cu was cleaned by electropolishing, H_2 reducing, pumping, and heating in an ultra-high vacuum. The measured H_2 amount was similar in all three cells. The authors only detected a monolayer of Cu_2O after 6 months of exposure at 50°C and a very low concentration of Cu species ($4 \mu\text{g}/\text{L}$ to $5 \mu\text{g}/\text{L}$) in the water. The authors could not establish whether the detected H_2 was a result of Cu corrosion, and concluded that the oxidation rate of Cu is very low in anoxic pure water.

Hedin, et al.,³⁰ published corrosion studies on copper samples with different structures and compositions, hydrogen in the bulk sample, and other impurities in anoxic water. Of the studied samples, only the oxygen-free and phosphorous-doped copper taken from an SKB canister sustained H_2 evolution for a few days. However, H_2 was not observed from the samples heated to 400°C in a vacuum. The researchers indicated that the evolved H_2 from the tests originated within the copper material and not from the corrosion process.

In the present study, the Cu foil used in H_2 evolution tests was only polished without any heat treatment for degassing. In all of the tests, H_2 was detected in the vapor phase and the amount of H_2 at the beginning was close to that after 3 months, which suggests that H_2 evolution was sustained during the test. However, the source of H_2 evolution was complicated by the stainless steel and nickel alloy autoclave material. At the test temperature of 80°C , the autoclave inner wall surface could also have corroded although the corrosion rate could be in nanometer per year range.³¹⁻³² The inner surface area of the autoclave was about $1,000 \text{ cm}^2$. If the corrosion rate was assumed to be $5 \text{ nm}/\text{y}$, the amount of H_2 generated by autoclave inner surface would be about $1.8 \times 10^{-5} \text{ mol}$ over 3 months, which is about $0.05 \text{ vol}\%$ and $0.015 \text{ vol}\%$, respectively, at 1 atm and 3 atm . This is close to the H_2 concentration detected from the vapor phase for tests in simulated granitic groundwater.

Previous studies³³⁻³⁵ show that hydrogen diffusivity decreases significantly with temperature. At the test temperature of 80°C , the diffusivity of hydrogen in Type 316 stainless steel and nickel alloy is in the range of $10^{-9} \text{ cm}^2/\text{s}$ to $10^{-11} \text{ cm}^2/\text{s}$. The wall thickness of the autoclave is about 7 mm . Based on the wall thickness and the diffusivity at 80°C , it would take about 15 y to $1,500 \text{ y}$ for the absorbed hydrogen to escape through the wall. In addition, the simulated granitic groundwater used in the work is not expected to depassivate the autoclave material to enhance hydrogen absorption. The combination of low hydrogen absorption efficiency and hydrogen diffusivity makes the chance of hydrogen escaping through the autoclave wall very small in the test duration from 3 months to 6 months. Hydrogen content analysis of the as-received and tested Cu foils indicates that they had the same level of hydrogen in the material. This suggests that the hydrogen detected in the tested specimen may be original hydrogen in the specimen and was not degassed or produced from the corrosion process. Thus the H_2 evolved from the test should have been contained in the autoclave. Nevertheless, because the amount of H_2 generated is so small, uncertainties of different techniques to determine the H_2 concentration and corrosion rate, and the complication from the autoclave material, the evolved H_2 cannot be simply associated with the Cu corrosion process.

CONCLUSIONS

❖ This study investigated copper open-circuit potential, corrosion rate, and hydrogen generation under anoxic conditions using a synthetic saline groundwater based on reference compositions for deep groundwaters in crystalline rocks of the Canadian Shield. The results indicate that the Cu open-circuit potential and corrosion rates in anoxic waters (less than 10 ppb of O_2) were very sensitive to the residual O_2

concentration in solution. The corrosion rates ranged from submicrometer to micrometers per year with increasing residual O₂ concentration level in parts per billion. Corrosion products were predominantly Cu₂O. Chlorine was present in corrosion products for tests exposed to synthetic saline groundwater, but further work is needed to assess the role of chloride anion in the corrosion process. H₂ also was found to be evolved from the tests, albeit in very small amounts. This small amount of H₂ evolved cannot be simply correlated to the Cu corrosion process because of the complication from the autoclave material.

ACKNOWLEDGMENTS

The authors gratefully acknowledge reviews by O. Pensado and D. Pickett. Appreciation is due to A. Ramos for assistance in preparing this paper. This paper describes work performed by the CNWRA for the NRC under Contract No. NRC-HQ-12-C-02-0089. The activities reported here were performed on behalf of the NRC Office of Nuclear Material Safety and Safeguards, Division of Spent Fuel Management. This paper is an independent product of the CNWRA and does not necessarily reflect the views or regulatory position of the NRC. The NRC staff views expressed herein are preliminary and do not constitute a final judgment or determination of the matters addressed or of the acceptability of any licensing action that may be under consideration at the NRC.

REFERENCES

1. F. King, *Corrosion* 69 (2013): p. 986-1011.
2. C.M. Lousada, I.L. Soroka, Y. Yagodzinsky, N.V. Tarakina, O. Todoshchenko, H. Hänninen, P.A. Korzhavii, M. Jonsson, *Sci. Rep.* 6 (2016): p. 1-8.
3. J.R. Scully, M. Edwards, "Review of the NWMO Copper Corrosion Allowance," Nuclear Waste Management Organization, NWMO TR-2013-04, Toronto, Canada, May 2013.
4. SKB, "Corrosion Calculations Report for the Safety Assessment SR-Site," Svensk Kärnbränslehantering AB, Swedish Nuclear Fuel and Waste Management Co., Technical Report TR-10-66, Stockholm, Sweden, 2010.
5. N. Taniguchi, M. Kawasaki, *J. Nucl. Mater.* 379 (2008): p. 154-161.
6. X. He, T. Ahn, J. McMurry, "Literature Review and Experiments on Waste Package Corrosion—Copper and Carbon Steel," U.S. Nuclear Regulatory Commission, ML16014A269, 2015.
7. X. He, T. Ahn, "Experiments on Corrosion of Copper and Carbon Steel Waste Containers—Progress Report for Fiscal Years 2015 and 2016," U.S. Nuclear Regulatory Commission, ML17003A453, 2017.
8. M. Pourbaix, *Atlas of Electrochemical Equilibria in Aqueous Solutions*, 2nd ed. (Houston, TX: NACE International, 1974).
9. P. Szakalos, G. Hultquist, G. Wikmark, *Electrochem. Solid-State Lett.* 10 (2007): p. C63-C67.
10. G. Hultquist, P. Szakalos, M.J. Graham, A.B. Belonoshko, G.I. Sproule, L. Grasjo, P. Dorogokupets, B. Danilov, T. Aastrup, G. Wikmark, G.-K. Chuah, J.-C. Eriksson, A. Rosengren, *Catal. Lett.* 132 (2009): p. 311-316.
11. G. Hultquist, M.J. Graham, P. Szakalos, G.I. Sproule, A. Rosengren, L. Grasjo, *Corros. Sci.* 53 (2011): p. 310-319.
12. G. Hultquist, M.J. Graham, O. Kodra, S. Moisa, R. Liu, U. Bexell, J.L. Smialek, *Corros. Sci.* 95 (2015): p. 162-167.
13. P. Fritz, S.K. Frappe, eds., *Saline Water and Gases in Crystalline Rocks*, Special Paper 33 (St. John's, Canada: Geological Association of Canada, 1987).
14. F. King, C. Lilja, K. Pedersen, P. Pitkänen, M. Vähänen, "An Update of the State-of-the-Art Report on the Corrosion of Copper Under Expected Condition in a Deep Geologic Repository," Swedish Nuclear Fuel and Waste Management Co, Technical Report TR-10-67, Stockholm, Sweden, December 2010.
15. J. McMurry, "Synthesis of Groundwater Test Solutions," Scientific Notebook 1228E (San Antonio, TX: Center for Nuclear Waste Regulatory Analyses, 2014), p. 1-39.
16. M. Gascoyne, "Reference Groundwater Composition for a Depth of 500 m in the Whiteshell Research Area—Comparison with Synthetic Groundwater WN-1," Atomic Energy of Canada Limited, Report AECL TR-463, Pinawa, Canada, 1988.
17. NWMO, "Used Fuel Repository Conceptual Design and Postclosure Safety Assessment in Crystalline Rock," Nuclear Waste Management Organization, Pre-Project Report NWMO TR-2012-16, Toronto, Canada, 2012.
18. J. McMurry, "Reference Water Compositions for a Deep Geologic Repository in the Canadian Shield," Ontario Power Generation, Report OPG 06819-REP-01200-10135-R01, Toronto, Canada, 2004.
19. Oakton Instruments, "Instruction Manual—DO 6—Economy Hand-Held Dissolved Oxygen Meter," Eutech Instruments Pte., Ltd., Rev. 0, 2004.
20. Hamilton, "VisiFerm™ DO Sensors Operating Instructions," Hamilton Bonaduz AG, 2014.
21. ASTM G102-89, "Standard Practice for Calculation of Corrosion Rates and Related Information from Electrochemical Measurements" (West Conshohocken, PA: ASTM International, 2004).
22. ASTM E1447-09, "Standard Test Method for Determination of Hydrogen in Titanium and Titanium Alloys by Inert Gas Fusion Thermal Conductivity/Infrared Detection Method" (West Conshohocken, PA: ASTM International, 2009).
23. ASTM G1, "Standard Practice for Preparing, Cleaning, and Evaluating Corrosion Test Specimens" (West Conshohocken, PA: ASTM International, 2003).
24. F. King, L. Ahonen, C. Taxén, U. Vuorinen, L. Werme, "Copper Corrosion Under Expected Conditions in a Deep Geologic Repository," Svensk Kärnbränslehantering AB, Swedish Nuclear Fuel and Waste Management Co., Technical Report TR-01-23, Stockholm, Sweden, 2001.
25. F. King, S. Watson, "Review of the Corrosion Performance of Selected Metals as Canister Materials for UK Spent Fuel and/or HLW," Nuclear Decommissioning Authority, QRA-1384J-1, 2010.
26. T. Kosec, A. Kranjc, B. Rosborg, A. Legat, *J. Nucl. Mater.* 459 (2015): p. 306-312.
27. M. Boman, R. Berger, Y. Andersson, M. Hahlin, F. Björefors, T. Gustafsson, M. Ottosson, *Corros. Eng. Sci. Technol.* 49 (2014): p. 431-434.
28. C. Cleveland, S. Moghaddam, M.E. Orazem, *J. Electrochem. Soc.* 161 (2014): p. C107-C114.
29. P. Wersin, S. Kastriot, J. Bruno, "Kinetic Modeling of Bentonite-Canister Interaction—Long-Term Predictions of Copper Canister Corrosion Under Oxidic and Anoxic Conditions," MBT, Tecnologia Ambiental, SKB TR 94-25, Cerdanyola, Spain, 1994.
30. A. Hedin, C. Lilja, J. Johansson, "Copper Corrosion in Oxygen Free Water—Status Report," SKB Document ID 1457600, 2014.
31. J.F. Grubb, T. DeBold, J.D. Fritz, "Corrosion of Wrought Stainless Steels," in *Corrosion: Materials*, eds. S.D. Cramer, B.S. Covino Jr., ASM Handbook, vol. 13B (Materials Park, OH: ASM International, 2005), p. 54-77.
32. P. Crook, "Corrosion of Nickel and Nickel-Base Alloys," in *Corrosion: Materials*, eds. S.D. Cramer, B.S. Covino Jr., ASM Handbook, vol. 13B (Materials Park, OH: ASM International, 2005), p. 228-251.
33. Y. Mine, T. Kimoto, *Corros. Sci.* 53 (2011): p. 2619-2629.
34. G.R. Caskey Jr., "Chapter 31: Hydrogen Effects in Stainless Steel," in *Hydrogen Degradation of Ferrous Alloys*, eds. R.A. Oriani, J.P. Hirth, M. Smialowski (Park Ridge, NJ: Noyes Publications, 1985).
35. A. Turnbull, G. Hinds, "Hydrogen Diffusion in Corrosion Resistant Alloys," CORROSION 2004, paper no. 469 (Houston, TX: NACE, 2004).